IEEE Access
Multidisciplinary ⋮ Rapid Review ⋮ Open Access Journal

Received 11 April 2024, accepted 24 April 2024, date of publication 29 April 2024, date of current version 6 May 2024.

Digital Object Identifier 10.1109/ACCESS.2024.3394447

RESEARCH ARTICLE

Wind Limitations at Madeira International Airport: A Deep Learning Prediction Approach

DÉCIO ALVES[1,2], DIOGO FREITAS[1,2,3], FÁBIO MENDONÇA[1,2], SHEIKH MOSTAFA[2], (Member, IEEE), AND FERNANDO MORGADO-DIAS[1,2], (Member, IEEE)

[1]Faculty of Exact Sciences and Engineering, University of Madeira, 9000-081 Funchal, Portugal
[2]Interactive Technologies Institute (ITI/LARSyS and ARDITI), 9020-105 Funchal, Portugal
[3]NOVA Laboratory for Computer Science and Informatics, NOVA LINCS, 7000-803 Lisbon, Portugal

Corresponding author: Décio Alves (decio.alves@iti.tecnico.ulisboa.pt)

This work was supported in part by ITI/Larsys—Funded by FCT (Fundação para a Ciência e a Tecnologia) projects: 10.54499/LA/P/0083/2020; 10.54499/UIDP/50009/2020 & 10.54499/UIDB/50009/2020 in part by Agência Regional para o Desenvolvimento da Investigação, Tecnologia e Inovação (ARDITI); and in part by the Portuguese Technical Engineering Order (OET).

ABSTRACT The unique geographical and topographical features of Madeira International Airport in Portugal significantly influence flight safety, primarily due to variable wind patterns. In this study, a machine learning approach is developed to predict runway operational statuses at Madeira International Airport, focusing on addressing wind-related challenges. To tackle this issue, a Deep Learning model is utilized. This model undergoes a particle swarm optimization process, resulting in one optimized model for each timestep, to provide minute-resolution predictions within a 20-minute timeframe. The training, validation, and testing phases for the optimized models were conducted using high-frequency wind data from Madeira International Airport. The main objective is to accurately predict the runway operational statuses, specifically whether the airport is open or closed for landing, take-off, or both. The models exhibit high performance, particularly in identifying operational conditions, reaching 99.93% precision, and a top accuracy of 94.35% predicting all runway status, underscoring their potential to enhance decision-making processes and operational efficiency under challenging weather conditions.

INDEX TERMS Machine learning, aviation meteorology, runway operations, Madeira Airport, flight safety.

I. INTRODUCTION

Weather, as a dominant factor in the domain of aviation, imposes limitations that significantly influence flight safety and operations [1]. Within the vast array of meteorological variables, wind, and visibility have consistently emerged as the most critical determinants, with adverse winds being the primary cause of weather-related accidents between 2000 and 2011 [1], [2], [3].

Situated in the subtropical eastern North Atlantic is the Madeira International Airport (MIA), a location that offers unique challenges. The intricate topography of the island exerts a profound influence on the climatic conditions experienced at the airport, result of the complex airflow pattern, exacerbated by the island's topography altering the prevailing wind regime from the North and Northeast sectors [4].

Given these conditions, MIA is subject to mandatory wind limitations. Exceeding these stipulated wind thresholds means that landing and take-off operations might not receive clearance from air traffic control, effectively bringing airport operations to a standstill [4], [5].

Evidence of the gravity of this situation can be gleaned from the data during the first 100 days of 2018, where adverse wind conditions impacted approximately 130 hours, affected 550 aircraft movements, and inconvenienced 80,000 passengers [4]. Considering tourism as the main source of Madeira's

The associate editor coordinating the review of this manuscript and approving it for publication was Yiqi Liu.

economy, with numerous tourists accessing the island via the airport [6], such disruptions wield a considerable negative economic impact. Further analysis of the data from 2015 to 2018 shows that the number of days impacted by wind limitations during the extended summer doubled compared to the period from 2010 to 2014, suggesting a rising trend in such events [4].

Considering this problem, the present study aims to develop a Machine Learning (ML) framework capable of predicting the operational status of the runway, specifically concerning the established wind limitations at MIA. Harnessing the capabilities of a Deep Learning (DL) approach, which has shown evidence of being highly effective in wind forecast [7], using a Long Short-Term Memory (LSTM) architecture to address a classification challenge [8], the main objective is to achieve minute-resolution predictions for a 20-minute extent [2]. Such predictive capabilities can significantly bolster decision-making processes for air traffic control at MIA, not only enhancing operational efficiency and safety of air traffic operations, but also facilitating more landing and takeoff operations, yielding financial savings for airlines, reducing the environmental pollution footprint, and minimizing the impact on passengers.

To the best of the author's knowledge, prior works have not focused specifically on predicting runway operational status based on wind characteristics as a classification problem through ML techniques. Although research such as that conducted by Cook et al. [9] has utilized a classification method using a Neural Network for predicting occurrences of wind gusts, most studies in this area predominantly lean towards regression models aimed at forecasting wind speed [2], [7]. This difference is crucial as regression models, while valuable for estimating the magnitude of wind speed, do not directly address the classification of operational statuses of runways under varying wind conditions that depend on wind speed, direction, gust intensity, the specific runway being utilized, and also vary depending on the sensor's location where these wind characteristics are measured. Nevertheless, there have been some explorations in applying ML classification approaches in aviation, particularly concerning airport or runway conditions and procedures, though unlinked with wind limits [10], [11], [12], [13], [14].

ML has also been explored to enhance airport operations by applying regression models to forecast runway acceptance rates [15]. Such predictions are intended to augment traffic efficiency and support human controllers [16] in their operational decisions. However, the primary emphasis of these studies has been on addressing issues related to airport configuration [15], [17], [18] rather than directly tackling the critical aspect of mandatory wind limitations that lead to immediate operational disruptions.

Considering this background, the main research question is whether ML can predict operational statuses at MIA concerning wind conditions, specifically within the parameters of predefined mandatory wind limitations.

The structure of this paper is as follows: Section II describes the data and methodologies used, and Section II-B presents the results and discussions. The research concludes with Section III, which outlines the derived conclusions.

II. MATERIALS AND METHODS

A. DATA COLLECTION

The data used in the present work, corresponding to the raw output of the wind sensors from MIA, was provided by NAV Portugal E.P.E., the air traffic service provider for Portugal. The MIA is located on the southeastern coast of Madeira Island, in the subtropical eastern North Atlantic [2], [19], as denoted in Figure 1, within a complex evolving terrain, particularly a significant mountain range, that affects the wind conditions at the runway [4].

As MIA has established mandatory wind limitations for take-off and landing operations to ensure the safety of flight operations, the wind thresholds were retrieved from the MIA Aeronautical Information Publication [4], [5].

The data acquisition equipment was a Väisälä wind set, model WA15, consisting of an Anemometer WAA151 and a Wind Vane WAV151, installed at four locations around MIA: ROSARIO at the short-final of runway 05, and three additional points labeled RWY05, MID, and RWY23 alongside the runway [5], as shown in Figure 1.

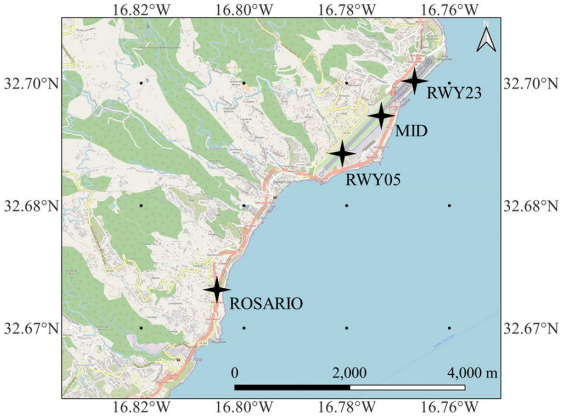

FIGURE 1. Location of Madeira International Airport and distribution of the examined wind sensors.

The dataset comprises raw observations, consisting of a Coordinated Universal Time (UTC) synched timestamp, wind speed in m/s, and wind direction in degrees, systematically captured at three-second intervals over a span of four years, beginning on 01-01-2018, and concluding on 31-12-2021 for each sensor. This accumulation results in a total of 168,230,063 points of valid data, representing 99.95% of the expected dataset. The invalid data, comprising periods of sensor maintenance or database errors where values consisted of non-valid wind information, was removed from the dataset. The data distribution is represented in Figure 2, where 2-A corresponds to the wind direction and 2-B to the wind speed records.

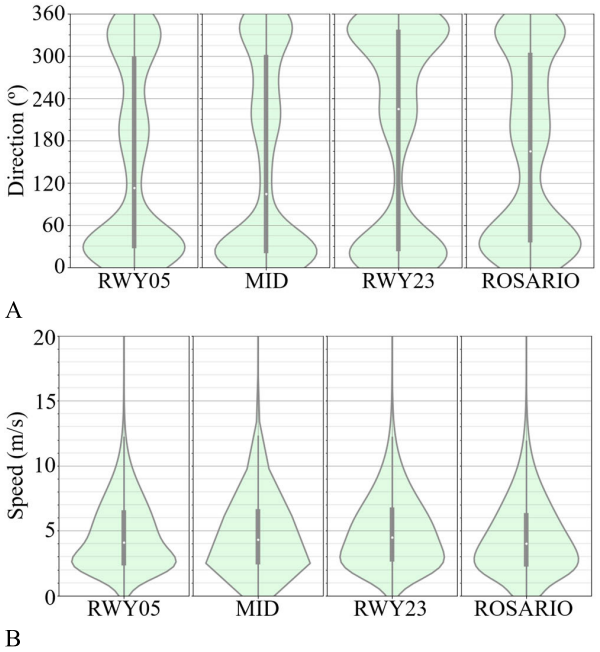

FIGURE 2. Violin plots of the wind speed and direction raw data where A presents the wind direction and B the wind speed for the entire dataset.

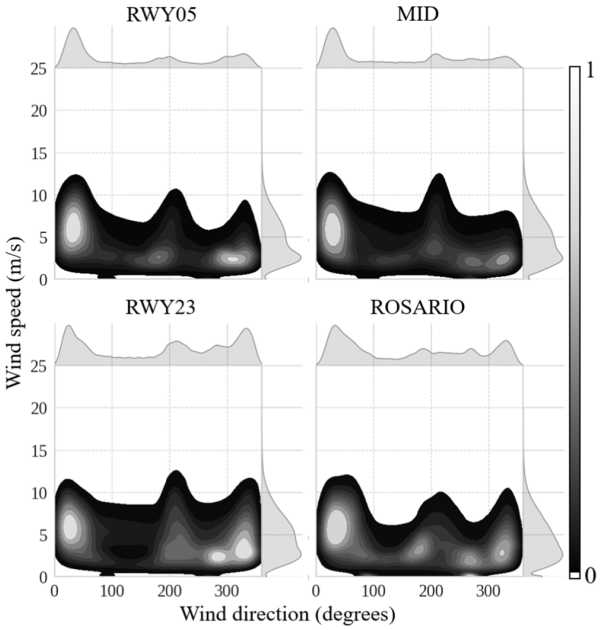

FIGURE 3. Joint distribution plots showing the probability density for wind speed and wind direction at RWY05, MID, RWY23, and ROSARIO.

The wind speed data from the four sensor locations showed average wind speeds of 4.66 m/s, 4.80 m/s, 4.92 m/s, and 4.49 m/s, for RWY05, MID, RWY23, and ROSARIO respectively. Standard deviations were 2.73 m/s at RWY05, 2.84 m/s at MID, 2.82 m/s at RWY23, and 2.84 m/s at ROSARIO, indicating moderate variability. The maximum wind speeds observed were 34.40 m/s (RWY05), 35.70 m/s (MID), 38.30 m/s (RWY23), and 28.40 m/s (ROSARIO), with a consistent minimum of 0 m/s at all locations. Additionally, wind direction data from all sensors predominantly showed northeast winds, with significant periods from the southeast.

Figure 3 presents a set of joint distribution plots depicting the Joint Probability Density (JPD) for wind speed and wind direction at RWY05, MID, RWY23, and ROSARIO.

For RWY05 and MID, the probability density coalesces into a distinct pattern, indicating that the most prevalent wind conditions are concentrated primarily in the northeastern quadrant, with wind speeds around 5 m/s. Conversely, the distributions for RWY23 and ROSARIO are broader, suggesting a more uniform distribution of wind speeds and directions. Although they share a peak probability at similar conditions to RWY05, both RWY23 and ROSARIO exhibit additional areas of high probability across multiple quadrants. Notably, RWY23 displays an increased likelihood of weaker winds, particularly in the northwest quadrant, where wind speeds are consistently below 5 m/s.

B. METHODS

The methodology employed in this research is divided into two primary stages: data preparation and label creation, with the subsequent development, application, and evaluation of a machine learning model for prediction.

1) DATA PREPARATION

The data preparation is essential to ensure the quality and reliability of the input for the predictive model [20]. In this study, the preparation of data involved two main steps. The first step included calculating the components $\vec{u}$ and $\vec{v}$ using the raw data collected every three seconds. The components were calculated by the equations below:

$$\vec{u_t} = -\omega_t \times \sin\left(\theta_t \times \left(\frac{\pi}{180}\right)\right) \quad (1)$$

$$\vec{v_t} = -\omega_t \times \cos\left(\theta_t \times \left(\frac{\pi}{180}\right)\right) \quad (2)$$

where the $\vec{u}$ component represents the wind's projection on the x-axis (East-West direction), while the $\vec{v}$ component corresponds to the projection on the y-axis (North-South direction). ω is the wind speed in m/s, θ is the wind direction in degrees, and t is the timestep indication.

Due to the high-frequency collection of wind data at three-second intervals, a two-minute moving average (MA) was then computed. More specifically, this process involved aggregating the data into 2-minute intervals, calculated every minute. This is mathematically represented as:

$$\mathrm{MA\ (p)} = \frac{1}{\mathrm{N}} \sum_{\mathrm{i}=\mathrm{J_t}+1}^{\mathrm{J_t}+\mathrm{N}} \mathrm{p_i\ for\ t} = 1, 2, \ldots, \frac{\mathrm{n}-\mathrm{N}+\mathrm{S}}{\mathrm{S}} \quad (3)$$

where p represents a specific feature in different points in time (t). N signifies the number of consecutive time periods, which is 40 in this context, and J_t represents the starting point of the window. J_t is defined as $J_t = S\,(t-1)$, where S denotes the step size, chosen to be 20 in this scenario.

A moving average was calculated, maintaining a high level of detail over time, and minimizing any potential delay or lag effects, while reducing the noise in the data and computational requirements. Furthermore, it aimed to decrease short-term fluctuations and align with the time frame of local operational decision-making [5], [21].

This feature engineering process was the second stage in preparing the data for analysis, and allowed to transform the original two features, which are wind speed and direction, into five final features for each sensor. Consequently, the final dataset includes the average wind speed ($\overline{\omega}$), average wind direction ($\overline{\theta}$), wind gust ($max\omega$), and the vector components of wind velocity ($\overline{\vec{u}}$ and $\overline{\vec{v}}$), i.e.:

$$\overline{\omega} = \text{MA}(\omega) \tag{4}$$

$$\overline{\vec{u}} = \text{MA}(\vec{u}) \tag{5}$$

$$\overline{\vec{v}} = \text{MA}(\vec{v}) \tag{6}$$

$$\overline{\theta} = \left(\arctan\left(\frac{\overline{\vec{u}}}{\overline{\vec{v}}}\right) + \pi\right) \times \frac{180}{\pi} \tag{7}$$

$$max\omega = \max_{i=J_t+1}^{J_t+N} \omega_i \text{ for } t = 1, 2, \ldots, \frac{n-N+S}{S} \tag{8}$$

It is important to note here that all features representing wind speed were then systematically converted to knots, conforming to the standardized unit for aeronautical reports [22] as adopted by the MIA. This conversion also aligns with the operational norms [5], [22], given that the wind limits for runway operations are also quantified and presented in knots.

The dataset was partitioned into three distinct temporal segments for model development. The training dataset encompassed records from 01/01/2018 at 00:02:00 to 31/12/2019 at 23:58:00, facilitating the initial phase of model learning by introducing patterns and behaviors from this period. Subsequently, the validation dataset, spanning 01/01/2020 at 00:02:00 to 31/12/2020 at 23:58:00, was employed to assess model performance and adjust hyperparameters iteratively during the training process. The final segment, the test dataset, covering 01/01/2021 at 00:02:00 to 31/12/2021 at 23:58:00, was reserved exclusively for evaluating the model's efficacy as novel, unseen data and used only after the completion of training. This structured approach ensured a sequential data flow from training through validation to testing, with each phase leveraging data from consecutive years. It is important to note that all results presented are derived from the test dataset, ensuring that performance metrics reflect the model's predictive accuracy and generalization capability on fresh data.

2) LABEL PREPARATION

The label preparation involved the categorization of operational statuses at MIA based on wind conditions, crucial for the prediction task. Labels were derived from the wind limitations outlined in the AIP, as detailed in Figure 4.

These operational limitations directly influence the airport's functioning, leading the Air Traffic Control (ATC) to withhold landing or take-off clearance when conditions fall outside these thresholds. The Touch Down Zone (TDZ) wind sensor, which varies depending on the active runway (either RWY05 or RWY23), was a focal point for label classification. A cross-section of the runway served as the boundary for determining the TDZ sensor: winds originating between sectors 320°-140° designated the RWY05 sensor as the TDZ, whereas winds from 140°-320° specified the RWY23 as the TDZ sensor.

Four operational states were established for MIA: Airport Open, Airport Closed for Take-off, Airport Closed for Landing, and Airport Closed for both Landing and Take-off. This classification is instrumental for the training of the predictive model, as it represents the target variable which reflects the airport's operational status.

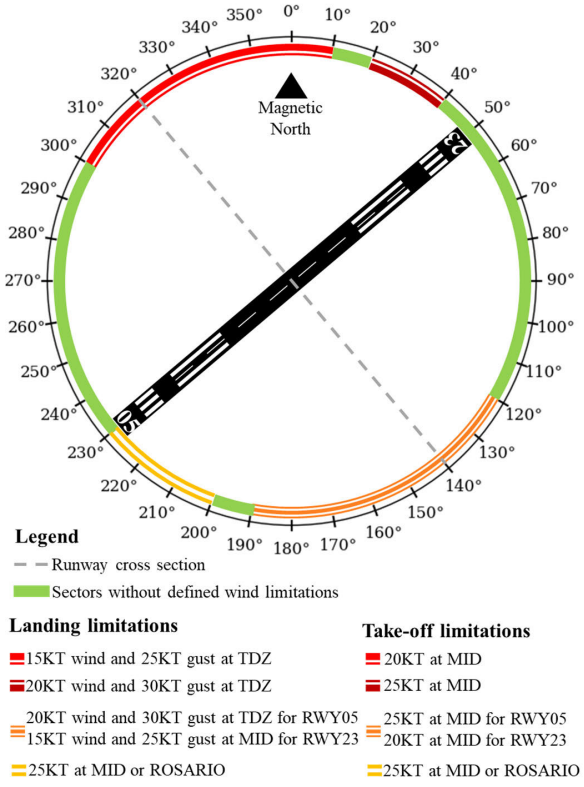

FIGURE 4. Wind limitations at MIA, showing the highest wind speed and gust allowed per angle.

3) MODEL DEVELOPMENT AND OPTIMIZATION

The utilization of a LSTM network in this study is primarily due to its proficiency in processing sequential data, making it particularly effective for recognizing wind patterns in time series [23]. An LSTM unit operates through a series of gates, namely the input gate, forget gate, and output gate, along with a cell state. These components collectively regulate the flow of information within each unit. The mathematical representation of the operations within an LSTM unit during a single time step is as follows:

$$i_t = \sigma\left(W_{xi}x_t + W_{hi}h_{t-1} + W_{ci}c_{t-1} + b_i\right) \tag{9}$$

$$f_t = \sigma\left(W_{xf}x_t + W_{hf}h_{t-1} + W_{cf}c_{t-1} + b_f\right) \quad (10)$$

$$c_t = f_t c_{t-1} + i_t \tanh\left(W_{xc}x_t + W_{hc}h_{t-1} + b_c\right) \quad (11)$$

$$o_t = \sigma\left(W_{xo}x_t + W_{ho}h_{t-1} + W_{co}c_t + b_o\right) \quad (12)$$

$$h_t = o_t \tanh\left(c_t\right) \quad (13)$$

where i_t, f_t, and o_t are the input, forget, and output gates at time t, respectively; c_t represents the cell state at time t; h_t represents the hidden state at time t; x_t is the input at time t; h_{t-1} and c_{t-1} are the hidden and cell states from the previous time step; W and b indicate the weights and biases associated with the different gates and states; σ is the sigmoid activation function and tanh represents the hyperbolic tangent activation function [24].

The architecture was based on the GrooveNet framework [8], [10], enhanced with two dropout layers to better prevent overfitting and improve the model's generalization capability [25] and denominated as Dropout-Enhanced GrooveNet, as illustrated in Figure 5.

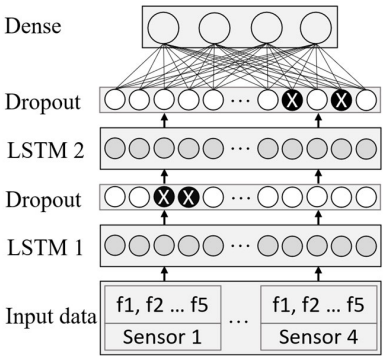

FIGURE 5. DE-GrooveNet model architecture.

Therefore, the DE-GrooveNet model architecture included an input layer with the shape of the dataset, two LSTM layers, and two Dropout layers with a rate of 0.2 to prevent overfitting. The final layer consisted of a fully connected dense layer with four neurons, using a SoftMax activation function, suitable for multi-class classification tasks [26].

The hyperparameters, namely the number of units in the LSTM layers, were optimized using a discrete binary variant of the Particle Swarm Optimization (PSO) [27], to determine the optimal number of units in its two LSTM layers, as it is a commonly used method for hyperparameter optimization [28].

This variant of PSO updated the velocity of each particle across iterations (i) and dimensions as described by

$$v_d^{(i+1)} = \omega^{(i)} v_d^{(i)} + c_1 r_1^{(i)}\left(p_d^{(i)} - x_d^{(i)}\right) + c_2 r_2^{(i)}\left(l_d^{(i)} - x_d^{(i)}\right) \quad (14)$$

where, ω represents the inertia weight parameter, while c_1 and c_2 are the cognitive and social weights, respectively. The terms r_1 and r_2 indicate two uniformly distributed pseudo-random numbers. The variables p and l are the personal best and the best positions found by the neighboring particles, respectively [27], [29].

Following the velocity computation, the position of each particle is updated in accordance with

$$x_d^{(i+1)} = \left\{ \begin{array}{ll} 1, & if\ \text{rand}() < \sigma\left(v_d^{(i+1)}\right) \\ 0, & otherwise \end{array} \right\} \quad (15)$$

where rand is a pseudorandom number from a uniform distribution on the interval $[0, 1]$, and σ denotes the sigmoid function.

The particles were organized in a ring topology, facilitating communication solely with two adjacent neighborhoods. This topology was selected to slow the convergence speed, a critical feature for multimodal complex optimization problems. The algorithm's exploration capabilities are enhanced by delaying convergence, reducing the likelihood of premature convergence and the risk of getting trapped in local minima. Additionally, the inertia weight parameter (ω) was adjusted following a negative non-linear time-varying approach, optimizing the algorithm's performance in navigating the solution space [27], [30]. The optimal and best performance model configuration was determined to include 200 units in the first LSTM layer and 76 units in the second LSTM layer.

Class weights were calculated to address imbalances in the training data, calculating the sum of each class (16), then the number of samples, the number of classes (17) (18), and the class weights (19), using

$$n_{class,i} = number\ of\ samples\ in\ i^{th}\ class \quad (16)$$

$$\text{total\_samples} = \text{number of samples in} y_{\text{train}} \quad (17)$$

$$n_{\text{classes}} = \text{number of classes in} y_{\text{train}} \quad (18)$$

$$\text{class weights} = \left\{ \text{i} : \frac{\text{total\_samples}}{\text{n}_{\text{classes}} \times \text{class\_sums}_{\text{i}}} \right\}_{\text{i}=0}^{\text{n}_{\text{classes}}-1} \quad (19)$$

where $y_{\text{train,class}}$ refers to the samples belonging to each class in the training set, total samples is the total number of samples in the training set, n_{classes} is the number of unique classes, *class_sums* is the sum of samples for the i-th class, and class_weights is a matrix where each key-value pair represents the class (key) and its corresponding weight (value), calculated as specified [31].

The model employed the Adam optimizer and categorical cross-entropy loss function, commonly used in multi-class classification approaches [32]. The Area Under the Precision-Recall Curve (AUC-PR) metric was used for evaluating performance, especially effective in imbalanced datasets [33].

An early stopping callback was integrated, monitoring AUC-PR on the validation data, and halting training after five epochs without improvement, to prevent overfitting and retain generalizability.

The training process was performed on the training dataset with the calculated class weights for up to 100 epochs, using a batch size of 128, and validation data to monitor performance.

To guarantee statistical robustness, a multi-run hold-out validation method was employed [34]. This involved repeating the training, validation and testing process ten times for each timestep, with each iteration using a unique random seed, totaling 200 simulations.

The presented results were obtained by analyzing metrics across all models. This involved looking at key performance indicators from the 200 simulations, across each of the ten iterations for every timestep. This method gives a clear view of the models' performance, ensuring the findings reflect consistent trends across different runs and conditions, rather than just a single instance.

4) MODEL APPLICATION AND EVALUATION

The LSTM model was used to forecast the operational status at MIA on a minute-by-minute basis, starting from one minute ahead of the current observation (T1) and continued up to 20 minutes into the future (T20) to offer sufficient lead time for operational decision-making support, based on the approach followed by Alves et al. [2].

This method aimed to provide a detailed and timely perspective on potential changes in airport operations. It was performed on the test data set, providing a real-world evaluation of new and unseen data by the model.

For each forecast point within this 20-minute frame, the model processed data from a one-hour input sequence. This duration, being three times longer than the prediction window, was selected to incorporate enough historical wind data, ensuring the model could effectively interpret and learn from recent wind patterns.

The key metrics employed to evaluate the model performance in predicting the operational status at MIA were Accuracy (Acc), Precision, Recall, and the F1-Score, aligning with state-of-the-art standard practices [35], [36], [37], as used by Muhammad et al. [38] for measuring the performance in a classification problem.

$$\text{Acc} = \frac{\text{Number of correct predictions}}{\text{Total number of predictions}} \times 100 \tag{20}$$

$$\text{Precision} = \frac{\text{TruePositives}}{(\text{TruePositives} + \text{FalsePositives})} \times 100 \tag{21}$$

$$\text{Recall} = \frac{\text{TruePositives}}{(\text{TruePositives} + \text{FalseNegatives})} \times 100 \tag{22}$$

$$\text{F1Score} = \frac{2(\text{Precision} \times \text{Recall})}{(\text{Precision} + \text{Recall})} \times 100 \tag{23}$$

To enhance the reliability of the LSTM model's performance evaluation, the model was executed ten times for each forecast within the 20-minute window. The calculated metrics were then averaged across these runs to minimize the impact of statistical outliers and ensure consistent results. Along with macro averages, weighted averages were also used to accurately reflect the varying frequencies of different operational statuses in the dataset, as it is generally practiced when dealing with unbalanced data [39], [40], thereby providing a balanced assessment of the model's predictive accuracy in varying conditions at MIA.

III. RESULTS AND DISCUSSION

A. AIRPORT OPERATIONAL DISRUPTIONS

Over the four-year period analyzed, MIA experienced a total of 20 days, 7 hours, and 38 minutes of operational closures due to wind conditions. A significant portion of this time, specifically 16 days, 2 hours, and 51 minutes, was attributed to closures for landing. This highlights the pronounced effect of wind on landing operations. In comparison, take-off operations were disrupted for 3 days, 1 hour, and 12 minutes. Furthermore, there were instances when landing and take-off operations were simultaneously affected, amounting to 1 day, 3 hours, and 35 minutes.

The influence of wind direction on these closures was markedly distinct. Winds from the southwest (RWY23) led to longer periods of closure, totaling 13 days, 11 hours, and 17 minutes, while northeast winds (RWY05) resulted in closures of 6 days, 20 hours, and 21 minutes.

Seasonal trends in wind disruptions were also evident, with July of 2020 and 2021 showing the highest annual frequency of closures, followed by May in 2019, indicating a pattern of increased closures in late spring and early summer. Notably, February 2018 and July 2020 were the months with the most significant disruptions, each experiencing a total closure time of 1 day, 19 hours, and 17 minutes.

B. MODEL PERFORMANCE

In analyzing the weighted average of the model's performance over 20 steps, several relevant trends emerged from assessing airport operational disruptions. The model's Precision, representing the quality of the positive predictions made by the model in specific instances, showed remarkable consistency across all steps, maintaining values above 98.98%. This high level of Precision indicates that the model was consistently reliable in its predictions when identifying specific operational disruptions due to wind conditions.

However, the model exhibited a gradual decline in Recall, which measures the ability to identify all relevant instances of disruptions. Starting from a high of 95.23%, the Recall decreased to 85.51% towards the final steps. This trend suggests that while the model remained accurate in its specific predictions, its capacity to capture all instances of disruptions slightly diminished over the steps. This could reflect changing environmental conditions or other external variables affecting the model's sensitivity to operational disruptions.

The F1-Score (23), a balanced measure that combines Precision and Recall, also exhibited a subtle decreasing trend, maintaining a close alignment with the consistently high Precision values. This pattern is depicted using boxplots in Figure 6, which aggregate the data from 10 simulations for each timestep. These boxplots provide a visual summary of the variability and central tendency of the F1-Score across multiple runs. This indicates that the model's overall performance was more influenced by its consistent accuracy in specific predictions than by its decreasing ability to capture every relevant instance.

TABLE 1. Results from test data predictions by time-step (presented as mean ± standard deviation).

Step	Label												Acc (%)
	Closed for landing			Closed for landing and take-off			Closed for take-off			Open			
	Precision (%)	Recall (%)	F1-Score (%)	Precision (%)	Recall (%)	F1-Score (%)	Precision (%)	Recall (%)	F1-Score (%)	Precision (%)	Recall (%)	F1-Score (%)	
1	34.43 ±14.05	61.90 ±08.50	41.88 ±08.15	21.29 ±08.84	67.34 ±16.73	29.99 ±07.84	03.73 ±00.95	70.89 ±13.68	07.05 ±01.70	99.95 ±00.02	94.72 ±00.93	97.26 ±00.49	94.35
2	27.37 ±06.59	63.91 ±03.58	37.78 ±06.63	16.65 ±05.11	74.56 ±07.86	26.59 ±06.04	02.61 ±00.52	64.04 ±12.03	05.00 ±00.99	99.96 ±00.01	93.29 ±00.89	96.51 ±00.47	92.94
3	29.21 ±08.93	58.87 ±05.04	38.21 ±06.40	18.44 ±08.34	70.69 ±12.25	27.58 ±08.39	02.76 ±00.65	69.19 ±11.95	05.31 ±01.23	99.95 ±00.02	93.45 ±01.04	96.59 ±00.55	93.06
4	24.90 ±04.70	62.50 ±02.54	35.34 ±04.74	18.77 ±06.03	64.56 ±14.97	27.39 ±04.34	03.06 ±00.47	67.06 ±11.42	05.85 ±00.87	99.95 ±00.01	93.82 ±00.70	96.79 ±00.37	93.45
5	25.17 ±05.60	60.07 ±04.48	34.99 ±05.06	15.93 ±06.22	72.64 ±11.14	25.12 ±07.42	02.48 ±00.30	64.84 ±15.47	04.77 ±00.54	99.96 ±00.01	92.86 ±00.88	96.28 ±00.47	92.48
6	30.53 ±10.61	56.15 ±06.97	37.99 ±07.92	13.48 ±04.40	75.47 ±12.13	22.24 ±05.64	02.54 ±00.49	61.04 ±09.34	04.86 ±00.89	99.94 ±00.01	93.51 ±00.60	96.61 ±00.32	93.08
7	25.46 ±05.28	54.70 ±10.46	33.94 ±04.93	11.97 ±04.58	77.04 ±09.90	20.16 ±06.02	02.20 ±00.67	62.51 ±11.07	04.24 ±01.25	99.93 ±00.07	92.19 ±01.75	95.89 ±00.94	91.76
8	24.06 ±08.51	56.11 ±03.29	32.76 ±07.46	11.87 ±04.20	76.65 ±12.49	19.98 ±05.71	02.88 ±00.90	60.96 ±16.46	05.46 ±01.62	99.94 ±00.02	93.32 ±01.49	96.51 ±00.79	92.90
9	23.45 ±03.61	57.81 ±06.02	33.10 ±03.32	12.59 ±03.56	73.67 ±07.66	21.14 ±04.70	02.89 ±01.13	62.58 ±08.88	05.49 ±02.03	99.94 ±00.02	93.33 ±01.31	96.52 ±00.69	92.92
10	25.49 ±09.46	60.32 ±07.33	34.28 ±08.15	15.53 ±07.61	66.82 ±16.60	23.19 ±07.39	02.54 ±00.88	63.67 ±15.83	04.86 ±01.65	99.94 ±00.02	92.43 ±02.04	96.03 ±01.09	92.05
11	30.06 ±10.69	51.74 ±05.25	36.59 ±06.31	15.04 ±06.83	68.23 ±11.30	23.42 ±06.47	02.55 ±00.64	73.90 ±09.15	04.93 ±01.20	99.93 ±00.03	92.65 ±01.56	96.15 ±00.83	92.21
12	23.40 ±07.09	58.27 ±07.51	32.41 ±05.83	17.88 ±06.07	62.51 ±12.33	26.66 ±05.96	02.37 ±00.42	71.99 ±12.74	04.58 ±00.79	99.95 ±00.01	91.76 ±01.28	95.68 ±00.70	91.39
13	22.17 ±06.15	54.98 ±04.99	30.98 ±05.63	11.21 ±04.33	67.44 ±22.03	18.58 ±06.64	02.58 ±00.75	66.17 ±10.90	04.96 ±01.42	99.94 ±00.01	92.49 ±01.39	96.06 ±00.75	92.06
14	24.45 ±06.18	56.90 ±06.15	33.50 ±05.25	13.65 ±05.81	65.20 ±13.75	21.76 ±07.35	02.24 ±00.45	70.20 ±10.69	04.34 ±00.86	99.95 ±00.01	91.71 ±01.08	95.65 ±00.58	91.32
15	21.10 ±05.62	57.45 ±05.75	30.29 ±05.56	14.06 ±02.28	64.36 ±10.23	22.82 ±02.94	02.45 ±00.49	71.43 ±07.83	04.73 ±00.93	99.95 ±00.01	91.67 ±02.29	95.61 ±01.27	91.29
16	23.47 ±06.65	55.40 ±13.74	31.10 ±04.93	14.91 ±06.31	68.45 ±14.17	23.16 ±07.00	02.46 ±00.57	64.18 ±09.64	04.73 ±01.05	99.91 ±00.09	92.60 ±00.79	96.12 ±00.44	92.18
17	27.05 ±06.38	50.87 ±03.83	34.91 ±05.17	12.09 ±06.22	73.60 ±14.34	19.53 ±06.96	01.89 ±00.50	65.05 ±12.90	03.67 ±00.95	99.94 ±00.01	91.39 ±01.21	95.47 ±00.66	90.95
18	26.76 ±05.63	53.14 ±05.51	35.01 ±03.80	10.66 ±04.38	75.15 ±13.64	18.00 ±06.10	02.20 ±00.52	59.66 ±16.01	04.23 ±00.99	99.92 ±00.02	92.78 ±00.85	96.22 ±00.45	92.33
19	23.64 ±06.93	49.92 ±06.79	31.06 ±04.69	14.87 ±10.21	64.29 ±24.62	19.23 ±04.97	02.19 ±00.38	69.40 ±14.73	04.24 ±00.73	99.92 ±00.05	91.76 ±01.51	95.66 ±00.81	91.31
20	24.49 ±07.29	55.03 ±06.10	32.90 ±05.73	12.48 ±04.48	70.42 ±10.89	20.56 ±05.64	02.40 ±00.68	61.99 ±12.10	04.62 ±01.25	99.93 ±00.02	92.66 ±01.17	96.15 ±00.63	92.23

The macro average of the performance achieved by the model in classifying different airport operational statuses across all time steps simulations shows that the model achieved high precision in identifying situations where the airport is operational, which is essential for maintaining efficient aviation operations, with a value of 98.98%. It also demonstrates robust recall across all categories, effectively identifying several true instances for both open and restricted operational states, with a weighted average of 98.31%.

Concurrently, the model sustains a commendable recall performance across diverse airport closure conditions, with 95.37%. This combination of high precision in critical scenarios alongside consistent recall efficacy underscores the model's proficiency in augmenting decision-making processes in aviation operations.

Table 1 shows the performance of the predictive models across 20 time-steps, focusing on different operational statuses at MIA. This tabulated data details the Precision, Recall, and F1-Score for each predicted status category: 'Closed for landing', 'Closed for landing and take-off', 'Closed for take-off', and 'Open', offering a perspective on the model's predictive capabilities over time for each type of operational disruption. It also presents the multi-class Acc for each timestep.

Analyzing the trends within this data, two patterns emerge and can be discerned. Initially, there is a trend of high performance in predicting the 'Open' status across all time steps,

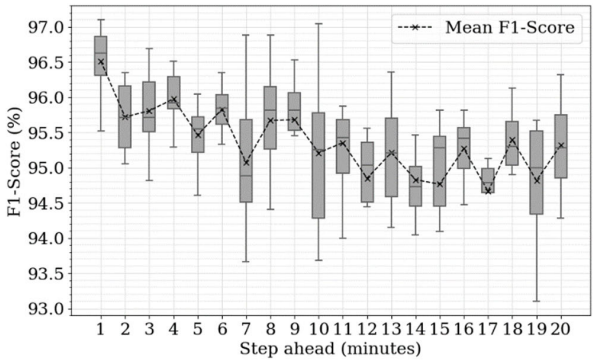

FIGURE 6. F1-Score weighted average variation over time step prediction. The dashed line represents the evolution of the mean value.

indicating the model's robust ability in accurately identifying normal operational periods. The second discernible pattern is a decrease in overall Acc over time.

This observed diminishing Acc over the time steps sequence indicates a potential decline in the model's proficiency in accurately forecasting operational statuses as it projects further into the future. It suggests that the model faces heightened challenges in predicting operational statuses that are more temporally distant, reflecting a possible increase in the complexity and more challenging problem for the model.

It is worth noting that the accuracy of the model is above the 90% mark in all predictions, varying from a top value of 94.35% at step 1 and a minimum of 90.95% at step 17.

An observation pertinent to the model's performance, delineated in Table 1, reveals that the precision metric for the ''closed for takeoff'' class attains the lowest values, with an average of 2.56%. This indicates a propensity of the model to predict this runway status when it is, in fact, not applicable. Nevertheless, the mean recall for the same class, quantified at 66.25%, suggests that the model successfully identifies over half of the actual occurrences of this runway status, assuring the model's potential to identify this class. The moderated precision for this condition could be attributed to the criteria for takeoff limitations being solely based on wind speed readings from a single sensor. In contrast, other statuses are determined based on both wind speed and gust measurements from multiple sensors, contingent upon the runway in use. Consequently, this could lead to the model's increased likelihood to overpredict the ''closed for takeoff'' status due to its comparatively minimal set of criteria.

In Figure 7, the confusion matrix for the model is presented [41], illustrating the distribution of predictions for the test dataset across all classes, exemplified by a single iteration with a one-step-ahead forecast.

The model accurately classifies 'open' (Op) class with an exactness of 95.35%. For the 'closed for landing' (CL) and 'closed for take-off,' (CT) classes the true positive rates are 71.00% and 57.79%, respectively, indicating the model's reliable predictive ability. In the scenario where runways are 'closed for landing and take-off,' (CLT) the model achieves

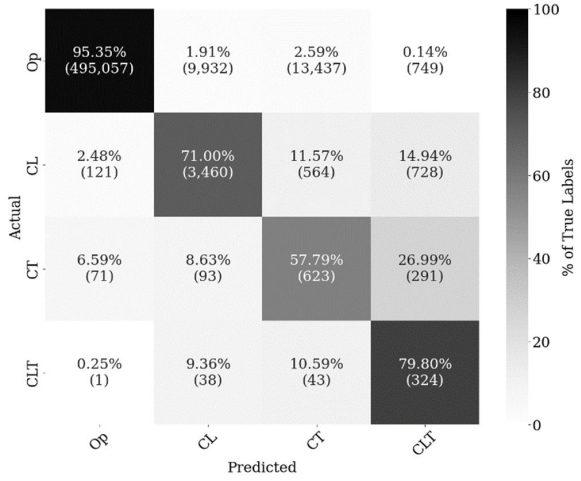

FIGURE 7. Confusion matrix for runway actual and predicted states at step 1.

a true positive rate of 79.80%. The matrix includes the absolute numbers of predictions for each category in parentheses, providing a clear picture of the model's classification distribution. The provided absolute numbers in parentheses detail the number of occurrences across different categories, demonstrating effectiveness in this context, of an unbalanced dataset.

The scatter plot in Figure 8 demonstrates a clear trend where the ''Open'' condition consistently achieves superior recall scores, above 90% across all steps, indicating better model performance in correctly identifying the true positives of this class.

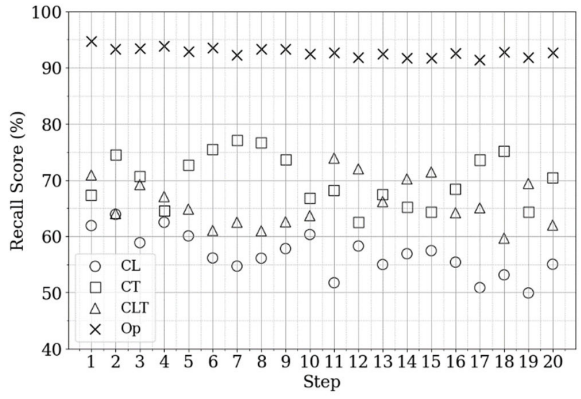

FIGURE 8. Scatter plot depicting the Recall Scores of all runway status, for all the predicted time steps.

Other conditions, while presenting some variability, generally maintain recall scores above 60%, reflecting a satisfactory level of performance. The ''Closed for landing'' category, despite being the most challenging for the Recall Score, still manages to stay mostly above the halfway mark, suggesting a decent model capability that could be further enhanced with targeted improvements. Overall, the results portray a model with a strong ability to correctly predict most

of the runway states correctly, particularly at the "Open" conditions.

IV. CONCLUSION

This research investigates the application of an optimized deep learning model for forecasting operational statuses of runways at Madeira International Airport, aiming to improve aviation safety and operational efficiency. This work is particularly relevant due to the distinctive topographical and wind conditions affecting the airport. The results affirmatively address the central question of the study, demonstrating the model's capability to predict operational statuses effectively. The model achieves a peak precision of 99.94% in identifying operational conditions, highlighting its potential utility in facilitating informed decision-making processes and augmenting operational efficiency under challenging weather conditions. The model accuracy was superior to 90%, with a peak of 94.35% when predicting one minute ahead. Since these outcomes originate from the test dataset, consisting of data that the model has not previously encountered and thus simulates real-world scenarios, it emphasizes the model's potential for practical application, demonstrating that it was not overfitted to the training dataset. In this way, the current approach serves as a first step baseline for runway wind limitations prediction, utilizing almost exclusively the existing sensors and infrastructures. This makes it well-suited for transposition to real world operation and decision-making support.

Addressing the study limitations, it is important to acknowledge the scope of data collection. The reliance on wind data primarily from sensors positioned along the runway might limit the comprehensiveness of environmental analysis. A broader spatial distribution of sensors could potentially yield a more holistic representation of wind patterns, thereby enhancing the predictive accuracy of the model.

Future research directions could encompass the incorporation of a more extensive meteorological dataset by expanding the sensor network to encompass a wider area.

In the same context, future research exploring different machine learning models and their architectures might provide insights into more effective ways of handling the diverse and complex wind conditions that impact operational decisions at airports like MIA. Such exploration is decisive for advancing the application of machine learning in aviation, particularly for operational planning and safety in airports situated in regions with challenging meteorological conditions. This study, therefore, represents an important initial step towards a broader and more nuanced application of advanced machine learning techniques in the field of aviation.

REFERENCES

[1] M. Schultz, S. Reitmann, and S. Alam, "Classification of weather impacts on airport operations," in *Proc. Winter Simul. Conf. (WSC)*, Dec. 2019, pp. 500–511, doi: 10.1109/WSC40007.2019.9004915.

[2] D. Alves, F. Mendonça, S. S. Mostafa, and F. Morgado-Dias, "Automated aviation wind nowcasting: Exploring feature-based machine learning methods," *Appl. Sci.*, vol. 13, no. 18, p. 10221, Sep. 2023, doi: 10.3390/app131810221.

[3] I. Gultepe et al., "A review of high impact weather for aviation meteorology," *Pure Appl. Geophys.*, vol. 176, no. 5, pp. 1869–1921, May 2019, doi: 10.1007/s00024-019-02168-6.

[4] M. Belo-Pereira and J. A. Santos, "Air-traffic restrictions at the Madeira international airport due to adverse winds: Links to synoptic-scale patterns and orographic effects," *Atmosphere*, vol. 11, no. 11, p. 1257, Nov. 2020, doi: 10.3390/atmos11111257.

[5] *AIP PORTUGAL LPMA AD 2*, document eAIP AIRAC 004-2023, Aeronaut. Inf. Publication, Lisbon, Portugal, Aug. 10, 2023.

[6] H. Viríssimo and J. Abrantes, "Is Madeira airport the beginning of a tourism experience on the island?" *Int. J. Islands Res.*, vol. 4, no. 1, pp. 35–39, 2023, doi: 10.57883/thij18(1)2022.30915.

[7] D. Alves, F. Mendonça, S. S. Mostafa, and F. Morgado-Dias, "The potential of machine learning for wind speed and direction short-term forecasting: A systematic review," *Computers*, vol. 12, no. 10, p. 206, Oct. 2023, doi: 10.3390/computers12100206.

[8] G. Van Houdt, C. Mosquera, and G. Nápoles, "A review on the long short-term memory model," *Artif. Intell. Rev.*, vol. 53, no. 8, pp. 5929–5955, Dec. 2020, doi: 10.1007/s10462-020-09838-1.

[9] N. J. Cook, "Automated classification of gust events in the contiguous USA," *J. Wind Eng. Ind. Aerodynamics*, vol. 234, Mar. 2023, Art. no. 105330, doi: 10.1016/j.jweia.2023.105330.

[10] A. Z. Cai, B. Lin Li, C. Y. Hu, D. W. Luo, and E. C. Lin, "Automated groove identification and measurement using long short-term memory unit," *Measurement*, vol. 141, pp. 152–161, Jul. 2019, doi: 10.1016/j.measurement.2019.03.071.

[11] A. D. Midtfjord and A. B. Huseby, "A machine learning approach to assess runway conditions using weather data," in *Proc. 31st Eur. Saf. Rel. Conf. (ESREL)*. Singapore: Research Publishing Services, 2021, pp. 833–840, doi: 10.3850/978-981-18-2016-8_474-cd.

[12] D. Chakraborty, S. Pal, and T. K. Nandi, "A machine learning based approach to detect birds over and around the runway before they strike the aircrafts," in *Proc. IEEE World Conf. Appl. Intell. Comput. (AIC)*, Jul. 2023, pp. 1–4, doi: 10.1109/aic57670.2023.10263907.

[13] E. V. Odisho, D. Truong, and R. E. Joslin, "Applying machine learning to enhance runway safety through runway excursion risk mitigation," *J. Aerosp. Inf. Syst.*, vol. 19, no. 2, pp. 98–112, Feb. 2022, doi: 10.2514/1.i010972.

[14] F. Herrema, R. Curran, S. Hartjes, M. Ellejmi, S. Bancroft, and M. Schultz, "A machine learning model to predict runway exit at Vienna airport," *Transp. Res. E, Logistics Transp. Rev.*, vol. 131, pp. 329–342, Nov. 2019, doi: 10.1016/j.tre.2019.10.002.

[15] Y. Wang and Y. Zhang, "Prediction of runway configurations and airport acceptance rates for multi-airport system using gridded weather forecast," *Transp. Res. C, Emerg. Technol.*, vol. 125, Apr. 2021, Art. no. 103049, doi: 10.1016/j.trc.2021.103049.

[16] Y. Nakamura, R. Mori, H. Aoyama, and H. Jung, "Modeling of runway assignment strategy by human controllers using machine learning," in *Proc. IEEE/AIAA 36th Digit. Avionics Syst. Conf. (DASC)*, Sep. 2017, pp. 1–7, doi: 10.1109/DASC.2017.8102099.

[17] A. Altinok, R. Kiran, B. Bue, and K. D. Bilimoria, "Modeling key predictors of airport runway configurations using learning algorithms," in *Proc. Aviation Technol., Integr., Oper. Conf.*, Jun. 2018, p. 3673, doi: 10.2514/6.2018-3673.

[18] A. Churchill, W. J. Coupe, and Y. C. Jung, "Predicting arrival and departure runway assignments with machine learning," in *Proc. AIAA AVIATION FORUM*. Reston, VA, USA: American Institute of Aeronautics and Astronautics, Aug. 2021, p. 2400, doi: 10.2514/6.2021-2400.

[19] P. M. A. Miranda, R. Tomé, L. Frois, M. Nogueira, J. M. R. Alves, V. Prior, R. Caldeira, and E. Dutra, "Speed-up of the Madeira tip jets in the ERA5 climate highlights the decadal variability of the Atlantic subtropics," *Quart. J. Roy. Meteorol. Soc.*, vol. 147, no. 734, pp. 679–690, Jan. 2021, doi: 10.1002/qj.3940.

[20] A. Jain, H. Patel, L. Nagalapatti, N. Gupta, S. Mehta, S. Guttula, S. Mujumdar, S. Afzal, R. Sharma Mittal, and V. Munigala, "Overview and importance of data quality for machine learning tasks," in *Proc. 26th ACM SIGKDD Int. Conf. Knowl. Discovery Data Mining*. NY, USA: ACM, Aug. 2020, pp. 3561–3562, doi: 10.1145/3394486.3406477.

[21] *Guide To Instruments and Methods of Observation (Observing Systems)*, 8th ed., World Meteorological Org., Geneva, Switzerland, 2018.

[22] *Annex 3—Meteorological Service for International Air Navigation (Amendment 79)*, 20th ed., Int. Civil Aviation Org., Montreal, QC, Canada, 2018. [Online]. Available: https://www.icao.int/airnavigation/IMP/Documents/Annex%203%20-%2075.pdf

[23] R. DiPietro and G. D. Hager, "Deep learning: RNNs and LSTM," in *Handbook of Medical Image Computing and Computer Assisted Intervention*. Amsterdam, The Netherlands: Elsevier, 2020, pp. 503–519, doi: 10.1016/B978-0-12-816176-0.00026-0.
[24] X. Shi, Z. Chen, H. Wang, D.-Y. Yeung, W.-K. Wong, and W. Woo, "Convolutional LSTM network: A machine learning approach for precipitation nowcasting," in *Proc. Adv. Neural Inf. Process. Syst.*, vol. 28, 2015, pp. 802–806.
[25] A. Omar and T. A. El-Hafeez, "Optimizing epileptic seizure recognition performance with feature scaling and dropout layers," *Neural Comput. Appl.*, vol. 36, no. 6, pp. 2835–2852, Feb. 2024, doi: 10.1007/s00521-023-09204-6.
[26] Y. Ren, P. Zhao, Y. Sheng, D. Yao, and Z. Xu, "Robust softmax regression for multi-class classification with self-paced learning," in *Proc. 26th Int. Joint Conf. Artif. Intell.* California, CA, USA: International Joint Conferences on Artificial Intelligence Organization, Aug. 2017, pp. 2641–2647, doi: 10.24963/ijcai.2017/368.
[27] J. Kennedy and R. C. Eberhart, "A discrete binary version of the particle swarm algorithm," in *Proc. IEEE Int. Conf. Syst., Man, Cybern. Comput. Cybern. Simulation*, Oct. 1997, pp. 4104–4108, doi: 10.1109/ICSMC.1997.637339.
[28] Y. Zhu, G. Li, R. Wang, S. Tang, H. Su, and K. Cao, "Intelligent fault diagnosis of hydraulic piston pump combining improved LeNet-5 and PSO hyperparameter optimization," *Appl. Acoust.*, vol. 183, Dec. 2021, Art. no. 108336, doi: 10.1016/j.apacoust.2021.108336.
[29] F. Mendonça, S. S. Mostafa, D. Freitas, F. Morgado-Dias, and A. G. Ravelo-García, "Multiple time series fusion based on LSTM: An application to CAP a phase classification using EEG," *Int. J. Environ. Res. Public Health*, vol. 19, no. 17, p. 10892, Sep. 2022, doi: 10.3390/ijerph191710892.
[30] D. Freitas, L. G. Lopes, and F. Morgado-Dias, "Particle swarm optimisation: A historical review up to the current developments," *Entropy*, vol. 22, no. 3, p. 362, Mar. 2020, doi: 10.3390/e22030362.
[31] W. Huang, G. Song, M. Li, W. Hu, and K. Xie, "Adaptive weight optimization for classification of imbalanced data," in *Proc. Intell. Sci. Big Data Eng.*, 2013, pp. 546–553, doi: 10.1007/978-3-642-42057-3_69.
[32] N. Gour and P. Khanna, "Multi-class multi-label ophthalmological disease detection using transfer learning based convolutional neural network," *Biomed. Signal Process. Control*, vol. 66, Apr. 2021, Art. no. 102329, doi: 10.1016/j.bspc.2020.102329.
[33] R. Avram, J. E. Olgin, and G. H. Tison, "The rise of open-sourced machine learning in small and imbalanced datasets: Predicting in-stent restenosis," *Can. J. Cardiol.*, vol. 36, no. 10, pp. 1574–1576, Oct. 2020, doi: 10.1016/j.cjca.2020.02.002.
[34] J. Levman, M. Jennings, P. Kabaria, E. Rouse, M. Nangaku, D. Berger, I. Gondra, E. Takahashi, and P. Tyrrell, "Hold-out validation for the assessment of stability and reliability of multivariable regression demonstrated with magnetic resonance imaging of patients with schizophrenia," *Int. J. Develop. Neurosci.*, vol. 81, no. 7, pp. 655–662, Nov. 2021, doi: 10.1002/jdn.10144.
[35] S. Orozco-Arias, J. S. Piña, R. Tabares-Soto, L. F. Castillo-Ossa, R. Guyot, and G. Isaza, "Measuring performance metrics of machine learning algorithms for detecting and classifying transposable elements," *Processes*, vol. 8, no. 6, p. 638, May 2020, doi: 10.3390/pr8060638.
[36] A. Humphrey, W. Kuberski, J. Bialek, N. Perrakis, W. Cools, N. Nuyttens, H. Elakhrass, and P. A. C. Cunha, "Machine-learning classification of astronomical sources: Estimating F1-score in the absence of ground truth," *Monthly Notices Roy. Astronomical Soc. Lett.*, vol. 517, no. 1, pp. L116–L120, Oct. 2022, doi: 10.1093/mnrasl/slac120.
[37] C. Goutte and E. Gaussier, "A probabilistic interpretation of precision, recall and F-score, with implication for evaluation," in *Proc. Adv. Inf. Retr.*, 2005, pp. 345–359, doi: 10.1007/978-3-540-31865-1_25.
[38] K. Muhammad, A. Ullah, J. Lloret, J. D. Ser, and V. H. C. de Albuquerque, "Deep learning for safe autonomous driving: Current challenges and future directions," *IEEE Trans. Intell. Transp. Syst.*, vol. 22, no. 7, pp. 4316–4336, Jul. 2021, doi: 10.1109/TITS.2020.3032227.
[39] A. Anand, G. Pugalenthi, G. B. Fogel, and P. N. Suganthan, "An approach for classification of highly imbalanced data using weighting and undersampling," *Amino Acids*, vol. 39, no. 5, pp. 1385–1391, Nov. 2010, doi: 10.1007/s00726-010-0595-2.
[40] R. Giuntini, F. Holik, D. K. Park, H. Freytes, C. Blank, and G. Sergioli, "Quantum-inspired algorithm for direct multi-class classification," *Appl. Soft Comput.*, vol. 134, Feb. 2023, Art. no. 109956, doi: 10.1016/j.asoc.2022.109956.
[41] R. N. Masolele, V. De Sy, M. Herold, D. Marcos, J. Verbesselt, F. Gieseke, A. G. Mullissa, and C. Martius, "Spatial and temporal deep learning methods for deriving land-use following deforestation: A pan-tropical case study using landsat time series," *Remote Sens. Environ.*, vol. 264, Oct. 2021, Art. no. 112600, doi: 10.1016/j.rse.2021.112600.

DÉCIO ALVES was born in Funchal, Portugal, in 1984. He received the B.S. degree in environmental sciences from Aberta University, Portugal, in 2015, and the M.S. degree in environmental engineering from European Atlantic University, Santander, Spain, in 2020. He is currently pursuing the Ph.D. degree with University of Madeira, Funchal. He is also a Researcher with the Interactive Technologies Institute (ITI/LARSyS). His research interests include environmental sciences, renewable energy, artificial intelligence, and meteorology.

DIOGO FREITAS was born in Funchal, Portugal, in 1996. He received the bachelor's degree in informatics engineering and the master's degree in mathematics and statistics from the Faculty of Exact Sciences and Engineering, University of Madeira, where he is currently pursuing the Ph.D. degree in informatics engineering, focusing on artificial intelligence, and conducts research on artificial intelligence models and optimization algorithms. He is also a Researcher with the Laboratory of Robotics and Engineering Systems, NOVA LINCS.

FÁBIO MENDONÇA was born in Funchal, Portugal, in 1990. He received the B.S. and M.S. degrees in electrical and telecommunications engineering from the University of Madeira, Portugal, in 2013 and 2016, respectively, and the Ph.D. degree from Instituto Superior Técnico, University of Lisbon, Portugal, in 2021. He is a Lecturer with the University of Madeira and a Researcher with the Interactive Technologies Institute–Laboratory for Robotics and Engineering Systems. His research interests include sleep monitoring, machine learning, and signal processing.

SHEIKH MOSTAFA (Member, IEEE) was born in Khulna, Bangladesh, in 1988. He received the B.S. (Eng.) degree from the University of Khulna, Bangladesh, in 2010, the M.S. degree from Khulna University of Engineering and Technology, Bangladesh, in 2012, and the Ph.D. degree from Instituto Superior Técnico, University of Lisbon, Portugal, in 2020. His research interests include signal and image processing, hardware implementations, and artificial neural networks.

FERNANDO MORGADO-DIAS (Member, IEEE) was born in Coimbra, Portugal, in 1971. He received the B.S. degree from the University of Aveiro, Portugal, in 1994, the M.S. degree from Joseph Fourier University, Grenoble, France, in 1995, and the Ph.D. degree from the University of Aveiro, in 2005.

He was a Lecturer with the Technical University of Setubal, Portugal. He is currently an Associate Professor with Aggregation with the University of Madeira. He is also a Researcher with the Interactive Technologies Institute. He is also the Director of the Ph.D. degree in electric engineering. His research interests include sleep monitoring, renewable energy, artificial neural networks, and FPGA implementations.

Dr. Morgado-Dias is a member of the Fiscal Council of the Portuguese Association of Automatic Control.